



Thermodynamic and dynamic responses of the hydrological cycle to solar dimming

Jane E. Smyth¹, Rick D. Russotto², and Trude Storelvmo¹

¹Department of Geology & Geophysics, Yale University, New Haven, Connecticut, USA

²Department of Atmospheric Sciences, University of Washington, Seattle, Washington, USA

Correspondence to: Jane Smyth (jsmyth@princeton.edu)

Abstract. The fundamental role of the hydrological cycle in the global climate system motivates thorough evaluation of its responses to climate change and mitigation. The Geoengineering Model Intercomparison Project (GeoMIP) is a global collaboration that aims to assess the climate impacts of solar geoengineering, a proposal to counteract global warming with a reduction of incoming solar radiation. We assess the mechanisms underlying the rainfall response to a simplified simulation of solar dimming in the suite of GeoMIP models and identify robust features. While solar geoengineering restores preindustrial temperatures, the global hydrology is altered. Tropical precipitation changes dominate the response across the model suite. The models indicate a range of possibilities for the hydrological response, and in most cases, both thermodynamic and non-thermodynamic mechanisms drive precipitation minus evaporation changes in the geoengineered simulations relative to the preindustrial. Shifts of the Hadley circulation cells cause greater rainfall anomalies than local changes in relative humidity or the Clausius-Clapeyron scaling of precipitation minus evaporation. The variations among models in the movement of the intertropical convergence zone highlights the need for cautious consideration and continued study before any implementation of solar geoengineering.

1 Introduction

Solar geoengineering has been suggested as a way to counter the effects of global warming induced by anthropogenic greenhouse gas emissions (e.g., Robock et al., 2009). By reducing incoming solar radiation, solar geoengineering would bring the climate with elevated concentrations of CO_2 into radiative balance. It compensates for a change in surface temperature from trapping of longwave radiation with a reduction of incoming shortwave radiation. Solar geoengineering is a controversial proposal, but should it come into favor due to continued greenhouse gas emissions, it is critical that the climate effects be understood before deployment (NRC, 2015).

The Geoengineering Model Intercomparison Project (GeoMIP) is intended to determine robust responses of the climate to various simulations of solar geoengineering, in experiments that range from simple representations of the solar dimming, to realistic representations of stratospheric aerosol emissions (Kravitz et al., 2010). The GeoMIP experiments are based on the Coupled Model Intercomparison Project Phase Five (CMIP5), which is a protocol for experiments using coupled atmosphere-ocean climate models (Table (1)). Preindustrial control simulations were run for 500 years after model spin-up, with preindus-



trial land cover and atmospheric compositions (Kravitz et al., 2010). The GeoMIP G1 experiment counteracts the forcing from quadrupled atmospheric CO_2 levels with a simple reduction of the solar constant across all wavelengths and spectra. The G1 experiment was run from the steady state preindustrial control run, followed by an abrupt quadrupling of CO_2 , and a simultaneous solar constant reduction for 50 years. The idealized nature of this simulation is conducive to multimodel comparison.

5 It superimposes two large and opposite climate forcings, which offset one another nearly completely in terms of global mean net radiation balance at the top of the atmosphere and near-surface atmospheric temperature, but do not totally cancel in their hydrological effects, especially on local scales (Kravitz et al., 2013c).

Thirteen fully coupled models participated in the G1 experiment (though only twelve are included in the present study), and they differ in their ocean, ice sheet, land surface and atmospheric components. The latter two components are particularly relevant for this study. Some, but not all models, feature dynamic vegetation distributions. The twelve models include a wide range of parametrizations and configurations, allowing for strong conclusions about robust climate responses that appear across models (Kravitz et al., 2013a).

10

The water cycle impacts agriculture, economies, as well as the welfare of ecosystems and human civilizations (IPCC, 2014). It is imperative to understand the effects of solar geoengineering on global hydrology, to evaluate whether such an approach to climate change mitigation is feasible or desirable. In order to help improve our understanding of this issue, we analyze the contributions of several different effects to changes in precipitation minus evaporation (P-E) in the GeoMIP G1 experiment. These include the thermodynamic scaling of P-E with temperature (Section 2.1), changes in relative humidity (Section 2.2), and changes in atmospheric circulation patterns (Section 2.3).

15

2 Analysis & Results

20 2.1 Thermodynamic Scaling of P-E

Surface heating increases the temperature and the evaporation rate, which increases the atmospheric moisture content, or specific humidity q (Trenberth, 1999). We have confidence about certain aspects of the hydrological cycle's response to greenhouse gas warming, particularly those tightly coupled to the increase in saturation vapor pressure with warming (Held and Soden, 2006). The Clausius-Clapeyron expression (Eq. (1)),

$$25 \quad \frac{d \ln e_s}{dT} = \frac{L}{RT^2} \equiv \alpha(T) \quad (1)$$

where R is the gas constant, L the latent heat of vaporization, and α is the Clausius-Clapeyron scaling factor, relates the derivative of the natural log of saturation vapor pressure e_s with respect to temperature T to temperature itself. At typical near-surface temperatures, saturation vapor pressure increases at $7\%K^{-1}$.

Precipitation minus evaporation determines the amount of runoff on land, and the salinity of the water column over ocean. Precipitation minus evaporation follows Clausius-Clapeyron scaling, as in Eq. (2), given three important assumptions (Held and Soden, 2006).

30

$$\delta(P - E) = \alpha \delta T (P - E) \quad (2)$$



First, it assumes small meridional gradients of temperature relative to P-E. Second, the relationship assumes no change in near-surface relative humidity between climate states. Third, it assumes that there is no change in the atmospheric flow. This thermodynamic scaling equation represents the component of P-E change driven directly by surface temperature perturbations.

P-E changes not captured by this scaling are driven by non-thermodynamic mechanisms, including changes in relative humidity

5 or atmospheric dynamics.

This project evaluates the extent to which the basic physical relation between saturation vapor pressure and temperature accounts for the climate response to a combination of large-magnitude forcings: greenhouse gas warming and solar dimming.

We investigate how well thermodynamic scaling predicts hydrologic changes in a geoengineered climate for each model by comparing the prediction using Eq. (2) to the annual and zonal mean P-E anomaly between G1 (years 11-50) and the
10 Preindustrial (all years) climate in the model simulations. We also consider the annual-mean global distribution of precipitation minus evaporation anomalies. In order to better understand the contribution of relative humidity changes to the P-E response, we also calculated an "extended scaling" adapted from Byrne and O’Gorman (2015). Our extended scaling includes the first two terms from Byrne and O’Gorman’s equation,

$$\delta(P - E) = \alpha \delta T (P - E) + \frac{\delta H_s}{H_s} (P - E) \quad (3)$$

15 where H_s is the relative humidity at the surface. The calculation takes local changes in H_s into account, but for the sake of simplicity it excludes changes in the horizontal gradients of H_s . We calculated the difference between the zonal mean P-E anomalies in the extended and simple scalings to quantify the influence of changes in H_s . We also calculated the difference between simulated P-E anomalies and the extended thermodynamic scaling, to isolate the role of dynamics in the simulated hydrological response. This analysis and the streamfunction analysis in section 2.3 were completed for a subset
20 of the ensemble due to limited functionality of the central GeoMIP model data server, the Earth System Grid Federation (ESGF).

The experimental design results in minimal temperature anomalies between G1 (years 11-50) and the preindustrial control (all years) (Fig. 1), but does not eliminate hydrological effects (Fig. 2). The ensemble mean change in P-E shows greater hydrological changes (up to 1 mm/day) in the tropics than at higher latitudes (Fig. 2). Figure (3), which separates the precipitation and evaporation changes from solar dimming, reveals that most of the spatial structure in the P-E anomaly (Fig. 4A) comes
25 from the precipitation change.

The thermodynamic scaling predicts virtually no change in global P-E patterns, since by experimental design the temperature anomaly is minimal between the G1 and preindustrial scenarios (Fig. 4B). Temperature anomalies between G1 and the preindustrial control show variations within 1 K, with some residual warming at high latitudes as a robust feature across the suite
(Fig. 1). The ensemble mean simulated precipitation minus evaporation deviates from the thermodynamic scaling by around
30 1.0 mm/day in the tropics, but due to the averaging of opposite responses among the models this understates the magnitude of the contrast between the scaling and the simulated P-E response (Fig. 2). The most pronounced differences occur in the tropics, where temperature anomalies are minimal compared to the high northern latitudes and thus cannot account for the hydrological



change. The exception to this is BNU-ESM, for which there is a pronounced P-E response at high latitudes, likely due to the poor compensation for the temperature response to quadrupled CO_2 levels in that model.

The ensemble mean reflects strong reductions in precipitation in the subtropics (Fig. 3). Previous research has suggested that this is a result of the nature of the G1 experiment forcing. Solar geoengineering might suppress tropical precipitation since the reduction in shortwave radiation cools the surface more than the mid-troposphere, increasing atmospheric stability and reducing convection (Bala et al., 2008). However, looking at the zonal patterns for individual models, there are stronger hydrological effects that cancel out in the ensemble mean (Fig. 4A). HadCM3, HadGEM2-ES, and CESM-Cam5.1-FV models show a northward shift in the ITCZ, while GISS-E2-R, Can-ESM2, and MIROC-ESM, demonstrate a southward shift. Annual mean anomalies in the zonal mean P-E exceed 0.6 mm/day in the GISS-E2-R and HadGEM2-ES simulations. In CCSM4, IPSL-CM5A-LR, and NorESM1-M models, the ITCZ narrows, with precipitation increasing at the equator and decreasing within 10 degrees latitude North and South. The precipitation results of the EC-EARTH model are un-physical and thus excluded from this analysis.

The deviations of the extended scaling from the simple scaling are less than 0.1 mm/day in all models (Fig. 4C). This demonstrates that local changes in relative humidity under solar dimming play a modest role in the zonal mean P-E response. Figure 4D indicates that most of the zonal mean P-E anomalies are not captured by the Clausius-Clapeyron scaling or by local relative humidity changes. We interpret this component of the hydrological response to be driven by atmospheric circulation changes. To better understand the influence of relative humidity changes on smaller spatial scales, we investigate the global distribution of H_s changes in the following section. We will then investigate the dynamical changes in the tropics in Section 2.3.

2.2 Relative Humidity

Relative humidity is the ratio of actual vapor pressure to saturation vapor pressure ($\frac{e}{e_s}$), or almost equivalently, specific humidity to saturation specific humidity ($\frac{q}{q_s}$). It can change with the evaporation rate or temperature, with the latter affecting the saturation vapor pressure as in Eq. (1). The near-surface atmosphere provides moisture to the free troposphere, where water vapor plays an important role in radiative transfer, the hydrological cycle, and climate sensitivity (Willett et al., 2010). The near-surface relative humidity parameter is also of interest in climate change studies for evaluating the risk of human heat stress, under both high and low H_s extremes (Sherwood et al., 2010; Souch and Grimmond, 2004).

The assumption of constant relative humidity in the simple thermodynamic scaling of P-E (Eq. (2)) relies on the availability of moisture. In a moisture-limited regime (i.e. over land) the specific humidity q may not increase proportionally with temperature, breaking the assumption of constant relative humidity. Under this circumstance, relative humidity adjustments would contribute to non-thermodynamic changes in the P-E between climate states. An observational study found decreasing surface relative humidity from 1998-2008 over low and midlatitude land areas due to inhomogeneities in surface heating and moisture availability (Simmons et al., 2010). While relative humidity has been found to be nearly constant in global warming simulations with high vertical resolution (Allen and Ingram, 2002), the assumption of constant H_s may not be sound when insolation rather than temperature is perturbed, as in the G1 experiment.



We consider the absolute changes in the relative humidity distribution to explain precipitation anomalies between G1 (years 11-50) and the preindustrial (all years) simulations unaccounted for by thermodynamic or dynamic mechanisms. Any changes in relative humidity between G1 and the preindustrial climate are due to changes in evaporation or evapotranspiration (Fig. 3), since saturation vapor pressure is maintained along with temperature in G1. In six of the eight models presented here, relative humidity is reduced over land and conserved over ocean (Fig. 5). The relative humidity reductions are largest over tropical South America and sub-Saharan Africa in the Can-ESM2, CCSM4, GISS-E2-R, HadGEM2-ES, IPSL-CM5A-LR, and NorESM1-M models. The reductions are up to 15% (0.15) in GISS-E2-R and HadGEM2-ES (calculated as the G1 relative humidity (%) minus the Preindustrial relative humidity (%)). The CO_2 physiological effect is included in the land models of eleven GeoMIP simulations, all but EC-Earth (Table (1)). In response to elevated ambient CO_2 concentrations, plants constrict their stomata, which reduces evapotranspiration in the high CO_2 simulations, including the G1 simulations (Kravitz et al., 2013c; Cao et al., 2010). In the global warming (abrupt4x CO_2) GeoMIP simulations, this effect is partially offset by the increased net primary productivity in a warmer world. However, in G1, this net primary productivity effect is muted by the reduction in insolation. Tilmes et al. (2013) found that the physiological response to G1 is qualitatively the same as for abrupt4x CO_2 . Biogeochemical cycling has been found to influence global precipitation as much as the radiative reduction itself (Fyfe et al., 2013).

Bala et al. (2008) investigate changes in global mean precipitation in a single climate model. They note a greater hydrological sensitivity to solar versus greenhouse forcing and attribute it to global energy budget constraints. Solar forcing heats the surface directly, while greenhouse forcing heats the troposphere. Changes in the insolation therefore have a greater effect on surface net radiation fluxes (i.e., latent and sensible heat fluxes change more than in the CO_2 case). When the downward shortwave flux decreases, the surface fluxes must respond, and in this case the latent heat flux dominates the response. Evaporation decreases, and precipitation follows. Bala et al. do not address how this global mean equilibrium constraint will manifest regionally, but our analysis (e.g. Fig 3) is consistent with this reasoning..

In the National Center for Atmospheric Research (NCAR) Community Land and Community Atmosphere Model, Cao et al. isolated the CO_2 physiological effect from a doubling of atmospheric CO_2 (2010). They reported patterns of reduced latent heat flux and relative humidity from this vegetative forcing that closely resemble those we observe in the GeoMIP suite, in Fig. 3 and Fig. 5. In the present study, since strong and significant reductions in relative humidity over land are largely constrained to regions with extensive vegetation in the form of boreal, temperate or tropical forests, we consider the biogeochemical effect of CO_2 to be the dominant cause of the relative humidity change. The role of these biogeochemical H_s changes is minimal in zonal mean climate (Fig. 4C) but could have significant influence at smaller spatial and temporal scales.

2.3 Dynamically Driven Precipitation

Large-scale meridional circulations are driven by energy gradients imposed by the uneven distribution of sunlight on Earth. The Hadley circulation cells are responsible for most of the poleward heat transport in the tropics, where the annual solar input is highest (Hill et al., 2015). The net energy flux of the Hadley circulation is in the flow direction of its upper branch (Held, 2001). The ascending motion of the Hadley cell drives the seasonally-migrating tropical rainfall known as the Intertropical



Convergence Zone (ITCZ), and there is evidence that its position is determined by meridional gradients in the vertically-integrated atmospheric energy budget (Shekar and Boos, 2016). The Hadley circulation is crucial for balancing global energy, so high-latitude temperature anomalies can drive shifts of the ITCZ (Yoshimori and Broccoli, 2008). The ITCZ is sensitive to interhemispheric energy contrasts set up by aerosols, clouds, or antisymmetric heating (Seo et al., 2014). A thorough analysis of Hadley circulation changes is a crucial outstanding task for understanding the hydrological response to solar geoengineering (Kravitz et al., 2013c). We will quantify changes to the Hadley circulation with the meridional streamfunction. The meridional streamfunction is derived from the continuity equation, and either \bar{v} or \bar{w} can be used to fully define the two-dimensional, overturning flow (Eq. (4)):

$$\Psi(\phi, p) = 2\pi a \cos\phi \int_0^p \bar{v} dp/g. \quad (4)$$

where ϕ is the latitude, p is pressure, a is the Earth's radius, \bar{v} is the meridional velocity, and g is gravity.

Changes in TOA energy fluxes influence the direction and strength of ITCZ shifts (Kang et al., 2008). Numerous studies have noted the strong relationship between ITCZ position and the hemispheric temperature contrast as well. The correlation between interhemispheric temperature contrasts and annual mean ITCZ position is a robust result and is related to extratropical energy transport (e.g., Broccoli et al., 2006; Toggweiler and Lea, 2010). Schneider et al. explain how this is consistent with an energetic framework: the hemisphere with the higher average temperature typically has a smaller meridional temperature gradient due to the near symmetry of tropical temperatures about the equator (2014). This corresponds to reduced poleward extratropical eddy transport in that hemisphere, and increased energy flux by the atmosphere across the equator and out of the hemisphere by the upper branch of the Hadley cell. The ITCZ is drawn towards the warmed hemisphere because moisture is transported in the opposite direction as energy by the Hadley cell. Therefore, we investigate the possibility that differing dynamical responses to solar dimming among the models are due to differences in the temperature restoration of the Northern and Southern hemispheres.

To discern the component of the precipitation change caused by changes in large scale atmospheric dynamics, we calculated the change in the Hadley circulation between the G1 (years 11-50) and Preindustrial Control (final 40 years) simulations. For each model, we computed the meridional streamfunction over this 40 year averaging period based on the modeled meridional wind vector, as in Eq. (4). We examined annual and seasonal mean dynamical changes to analyze the changes in the zonal mean hydrological cycle. To better interpret the dynamical changes, we assessed the change in the interhemispheric temperature contrast between G1 and the Preindustrial for each model by calculating area-weighted hemispheric averages of the surface temperature, averaged over a 40 year period (years 11-50 of G1 and 1-40 of the Preindustrial Control). The ITCZ shift between G1 and the Preindustrial is defined as the shift of the precipitation centroid. This is the latitude between 15 degrees North and 15 degrees South at which half the precipitation is to the north and half is to the south.

The annual mean Hadley circulation changes vary in magnitude and direction amongst the GeoMIP ensemble members and contribute to dynamic moistening and drying. The meridional streamfunction plots suggest that the northward (HadGEM2-ES) and southward (GISS-E2-R, MIROC-ESM) ITCZ shifts, characterized by counterclockwise or clockwise tropical anomalies



respectively, are dynamically driven (Fig. 6). The anomalous ascent at the equator in CCSM4 and NorESM1-M accounts for the narrowing of the ITCZ noted in the zonal mean P-E figure. The mean circulation does not seem to provide a dynamical basis for the annual mean constriction of the ITCZ in the MPI-ESM-LR and IPSL-CM5A-LR models, in which anomalies are less than $10 \text{ kgs}^{-1} \times 10^9$. Small changes in the latitudinal range and strength of the Hadley circulation and associated precipitation have large local implications, especially on subannual scales (Kang et al., 2009). We find that summer (July-August-September, or JAS) and winter (December-January-February, or DJF) meridional streamfunction anomalies are in every model stronger than the annual mean, since opposite responses in different seasons average out in the annual mean (not shown). In HadGEM2-ES, for example, the JAS meridional mass flux anomaly exceeds $40 \text{ kgs}^{-1} \times 10^9$. On the opposite extreme, the IPSL-CM5A-LR model JAS and DJF mass flux anomalies are below $15 \text{ kgs}^{-1} \times 10^9$.

We find that the shifts of annual mean tropical rainfall in the models are correlated with the interhemispheric surface temperature contrasts ($r = 0.638$, Fig. 7). Models with higher annual mean surface temperatures in the Northern Hemisphere under geoengineering tend to display northward shifts of the ITCZ. This is consistent with previous research that shows a strong relationship between the ITCZ position and the hemispheric temperature contrast (e.g., Kang et al., 2008; Frierson and Hwang, 2012). Despite the hemispherically symmetric forcing induced by solar dimming, the ensemble mean residual high-latitude warming is larger in the Arctic than in the Antarctic (Fig. 1), and in 9 out of 11 models the northern hemisphere is warmed relative to the southern hemisphere after geoengineering (Fig. 7). This suggests that there could be an intriguingly close relationship between the degree of Arctic warming amplification and the tropical hydrological response to geoengineering in models. The relationship between ITCZ shifts and energy transport in G1 will be further explored in a future study.

3 Conclusions

There is not a single mechanism driving the P-E changes in climate model simulations of uniform solar dimming. Rather, a combination of thermodynamic scaling of precipitation minus evaporation, relative humidity changes, and Hadley circulation shifts contribute to the hydrological response, to different extents in each model. In the 11-member ensemble, there is variability not only in the spatial distribution of precipitation changes, but also in the underlying causes. P-E changes were generally driven more by dynamics than by relative humidity changes or thermodynamics.

The models can be divided into three groups characterized by different precipitation responses to geoengineering: either a southward shift, northward shift, or narrowing of the ITCZ. Our results support that changes in tropical dynamics, namely shifts of the Hadley circulation, are in part responsible for these alterations to the P-E distribution. In a previous study, convection scheme parameters were determinative of the tropical precipitation response to extratropical forcings (Kang et al., 2009). The partitioning of cross-equatorial fluxes between atmospheric and oceanic components is also important for the resulting ITCZ shift, so differences in the oceanic component of the models could emerge as significant (Kang et al., 2008).

We also present evidence that land-sea contrasts in evaporation rates, resulting in land-sea contrasts in relative humidity anomalies, contribute to changes in P-E with solar dimming. We propose that these relative humidity changes are related to the effect of CO_2 on the stomatal conductance in plants.



This study demonstrates that tropical precipitation is sensitive to solar perturbations and would be altered by an implementation of solar geoengineering. The basis of this alteration is primarily dynamical. Based on our inter-model comparison, there is substantial uncertainty regarding the nature of the tropical precipitation response, in terms of the direction and strength of the ITCZ shift, as well as its variation on seasonal time scales. We present evidence that residual warming of one hemisphere relative to the other under geoengineering draws annual mean tropical rainfall into that hemisphere. The ramifications of this result on seasonal timescales requires further study. Our findings strengthen the conclusion that solar geoengineering cannot restore preindustrial conditions in terms of P-E patterns, a fundamental aspect of climate.

Author contributions. T. Storelvmo designed research and J.E. Smyth performed the analysis. J.E. Smyth and T. Storelvmo interpreted results, and J.E. Smyth wrote the manuscript with input from the coauthors. R.D. Russotto contributed Figure 7 and assisted with the preparation of the manuscript text.

Acknowledgements. We thank the climate modeling groups for participating in the Geoengineering Model Intercomparison Project and for making their data available. In particular we thank Dr. Ben Kravitz and the scientists managing the Earth System Grid Federation for facilitating data access. T. Storelvmo was supported by NSF under grant 1352417. J.E. Smyth was supported by the Karen Von Damm '77 Undergraduate Research Fellowship from the Yale University Department of Geology & Geophysics. R.D. Russotto was supported by the U.S. Department of Defense (DoD) through the National Defense Science and Engineering Graduate Fellowship (NDSEG) Program..



References

- Allen, M. R. and Ingram, W. J.: Constraints on future changes in climate and the hydrologic cycle, *Nature*, 419, 224–232, 2002.
- Bala, G., Duffy, P., and Taylor, K.: Impact of geoengineering schemes on the global hydrological cycle, *PNAS*, 105, 7664–7669, 2008.
- Broccoli, A. J., Dahl, K. A., and Stouffer, R. J.: Response of the ITCZ to Northern Hemisphere cooling, *Geophysical Research Letters*, 33, doi:10.1029/2005GL024546, <http://dx.doi.org/10.1029/2005GL024546>, 101702, 2006.
- Byrne, M. P. and O’Gorman, P. A.: The Response of Precipitation Minus Evapotranspiration to Climate Warming: Why the “Wet-Get-Wetter, Dry-Get-Drier” Scaling Does Not Hold over Land, *Journal of Climate*, 28, 8078–8092, doi:10.1175/JCLI-D-15-0369.1, 2015.
- Cao, L., Bala, G., Caldeira, K., Nemani, R., and Ban-Weiss, G.: Importance of carbon dioxide physiological forcing to future climate change, *Proceedings of the National Academy of Sciences*, 107, 9513–9518, doi:10.1073/pnas.0913000107, 2010.
- 10 Frierson, D. and Hwang, Y.-T.: Extratropical Influence on ITCZ Shifts in Slab Ocean Simulations of Global Warming, *Journal of Climate*, 25, 720–733, doi:10.1175/JCLI-D-11-00116.1, 2012.
- Fyfe, J., Cole, J., Arora, V., and Scinocca, J.: Biogeochemical carbon coupling influences global precipitation in geoengineering experiments, *Geophys. Res. Letters*, 40, 651–655, 2013.
- Held, I.: The Partitioning of the Poleward Energy Transport between the Tropical Ocean and Atmosphere, *Journal of the Atmospheric Sciences*, 58, 943–948, 2001.
- 15 Held, I. and Soden, B.: Robust responses of the hydrological cycle to global warming, *Journal of Climate*, 19, 5686–5699, 2006.
- Hill, S., Ming, Y., and Held, I.: Mechanisms of Forced Tropical Meridional Energy Flux Change, *Journal of Climate*, 28, 1725–1742, 2015.
- IPCC: *Climate Change 2014: Impacts, Adaptation, and Vulnerability. Part A: Global and Sectoral Aspects*, p. 1132, Cambridge University Press, Cambridge, United Kingdom and New York, NY, USA, 2014.
- 20 Kang, S., Held, I., Frierson, D., and Zhao, M.: The Response of the ITCZ to Extratropical Thermal Forcing: Idealized Slab-Ocean Experiments with a GCM, *Journal of Climate*, 21, 3521–3532, 2008.
- Kang, S., Frierson, D., and Held, I.: The Tropical Response to Extratropical Thermal Forcing in an Idealized GCM: The Importance of Radiative Feedbacks and Convective Parameterization, *Journal of the Atmospheric Sciences*, 66, 2812–2827, 2009.
- Kravitz, B., Robock, A., Boucher, O., Schmidt, H., and Taylor, K.: Specifications for GeoMIP experiments G1 through G4, Available online at <http://climate.envsci.rutgers.edu/GeoMIP/docs/specificationsG1G4.pdf> [accessed April 2016], 2010.
- 25 Kravitz, B., Caldeira, K., Boucher, O., Robock, A., Rasch, P. J., Alterskjær, K., Karam, D. B., Cole, J. N. S., Curry, C. L., Haywood, J. M., Irvine, P. J., Ji, D., Jones, A., Kristjánsson, J. E., Lunt, D. J., Moore, J. C., Niemeier, U., Schmidt, H., Schulz, M., Singh, B., Tilmes, S., Watanabe, S., Yang, S., and Yoon, J.-H.: Climate model response from the Geoengineering Model Intercomparison Project (GeoMIP), *JGR: Atmospheres*, 118, 8320–8332, 2013a.
- 30 Kravitz, B., Rasch, P. J., Forster, P. M., Andrews, T., Cole, J. N. S., Irvine, P. J., Ji, D., Kristjánsson, J. E., Moore, J. C., Muri, H., Niemeier, U., Robock, A., Singh, B., Tilmes, S., Watanabe, S., and Yoon, J.-H.: An energetic perspective on hydrological cycle changes in the Geoengineering Model Inter-Comparison Project, *JGR: Atmospheres*, 118, 13,087–13,102, 2013c.
- NRC: *Front Matter. Climate Intervention: Reflecting Sunlight to Cool Earth*, Washington, DC: The National Academies Press, doi:10.17226/18988, 2015.
- 35 Robock, A., Marquardt, A., Kravitz, B., and Stenchikov, G.: Benefits, risks, and costs of solar geoengineering, *Geophysical Research Letters*, 36, 2009.
- Schneider, T., Bischoff, T., and Huag, G.: Migrations and dynamics of the intertropical convergence zone, *Nature Review*, 513, 45–53, 2014.



- Seo, J., Kang, S., and Frierson, D.: Sensitivity of Intertropical Convergence Zone Movement to the Latitudinal Position of Thermal Forcing, *Journal of Climate*, 27, 3035–3042, 2014.
- Shekar and Boos: Improving Energy-Based Estimates of Monsoon Location in the Presence of Proximal Deserts, *Journal of Climate*, 29, 2016.
- 5 Sherwood, S. C., Ingram, W., Tsushima, Y., Satoh, M., Roberts, M., Vidale, P. L., and O’Gorman, P. A.: Relative humidity changes in a warmer climate, *Journal of Geophysical Research: Atmospheres*, 115, doi:10.1029/2009JD012585, 2010.
- Simmons, A. J., Willett, K. M., Jones, P. D., Thorne, P. W., and Dee, D. P.: Low-frequency variations in surface atmospheric humidity, temperature, and precipitation: Inferences from reanalyses and monthly gridded observational data sets, *Journal of Geophysical Research: Atmospheres*, 115, doi:10.1029/2009JD012442, 2010.
- 10 Souch, C. and Grimmond, C.: Applied climatology:heat waves’, *Progress in Physical Geography*, 28, 599–606, 2004.
- Tilmes, S., Fasullo, J., Lamarque, J.-F., Marsh, D. R., Mills, M., Alterskjær, K., Muri, H., Kristjánsson, J. E., Boucher, O., Schulz, M., et al.: The hydrological impact of geoengineering in the Geoengineering Model Intercomparison Project (GeoMIP), *Journal of Geophysical Research: Atmospheres*, 118, 2013.
- Toggweiler, J. R. and Lea, D. W.: Temperature differences between the hemispheres and ice age climate variability, *Paleoceanography*, 25, doi:10.1029/2009PA001758, <http://dx.doi.org/10.1029/2009PA001758>, pA2212, 2010.
- 15 Trenberth, K.: Atmospheric Moisture Recycling: Role of Advection and Local Evaporation, *Journal of Climate*, 12, 1368–1381, 1999.
- Willett, K., Jones, P., Thorne, P., and Gillett, N.: A comparison of large scale changes in surface humidity over land in observations and CMIP3 general circulation models, *Environmental Research Letters*, 5, 025 210, 2010.
- Yoshimori and Broccoli: Equilibrium Response of an Atmosphere–Mixed Layer Ocean Model to Different Radiative Forcing Agents: Global and Zonal Mean Response, *J. Atmos. Sci.*, 21, 4399–4423, 2008.
- 20

FIGURES

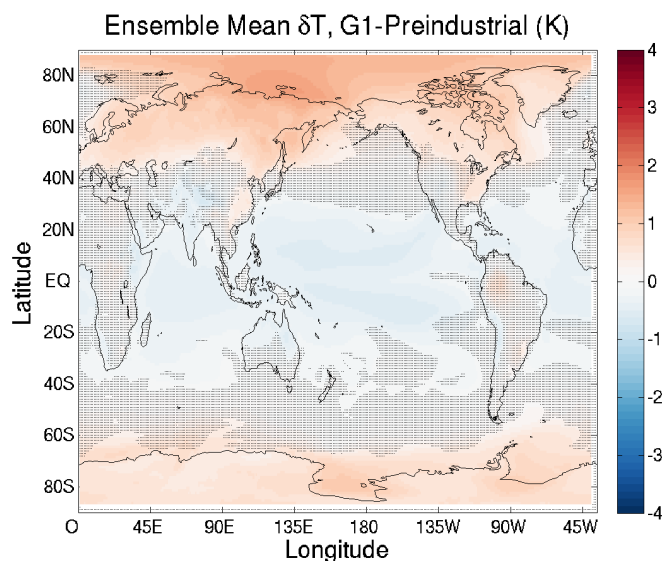


Figure 1. The annual mean distribution of near-surface atmospheric temperature anomalies (K) between G1 (years 11-50) and the Preindustrial Control (all years). Stippling denotes regions where fewer than 66% of the twelve ensemble members agree on the sign of the change.

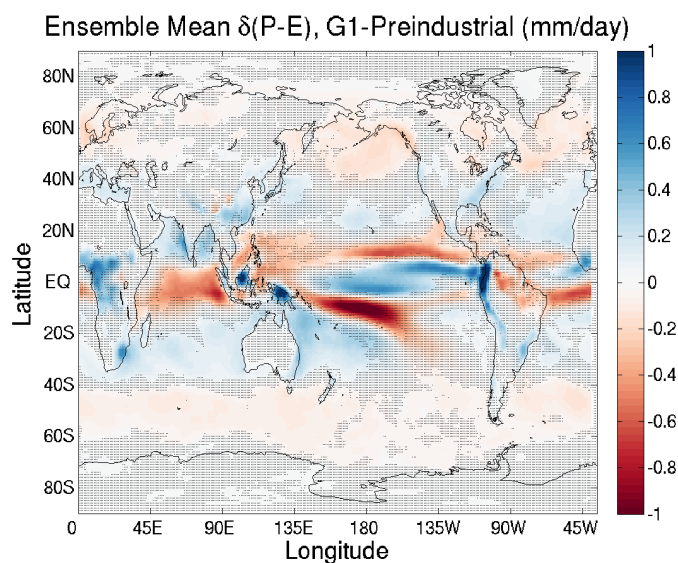


Figure 2. The annual mean distribution of precipitation minus evaporation rate anomalies (mm/year) between G1 (years 11-50) and the Preindustrial Control (all years), averaged among eleven models (EC-Earth excluded due to unphysical result). Stippling indicates where fewer than 64% of models agree on the sign of the change.

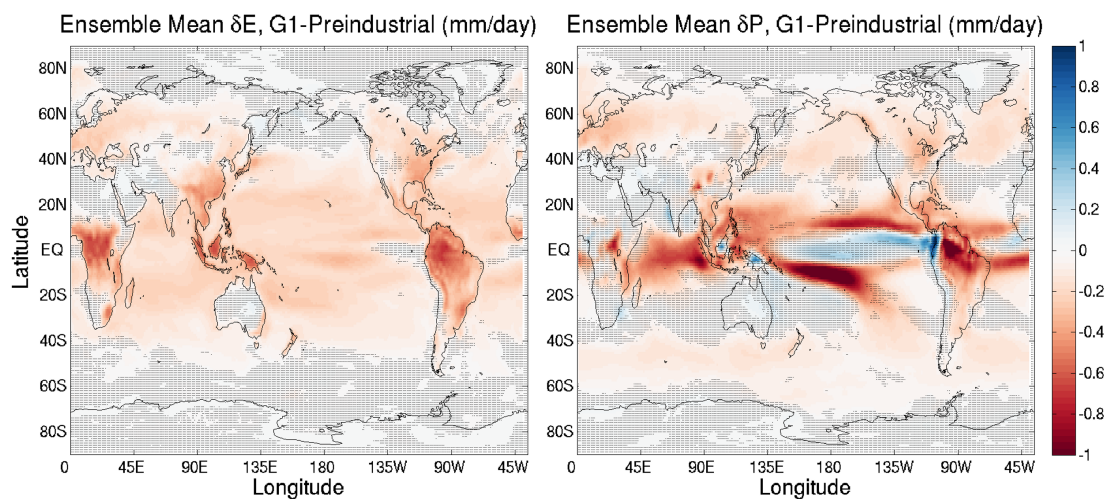


Figure 3. The annual mean distribution of evaporation (left panel) and precipitation (right panel) rate anomalies (mm/year) between G1 (years 11-50) and the Preindustrial Control (all years), averaged among eleven models (EC-Earth excluded due to unphysical result). Stippling indicates where fewer than 64% of models agree on the sign of the change.

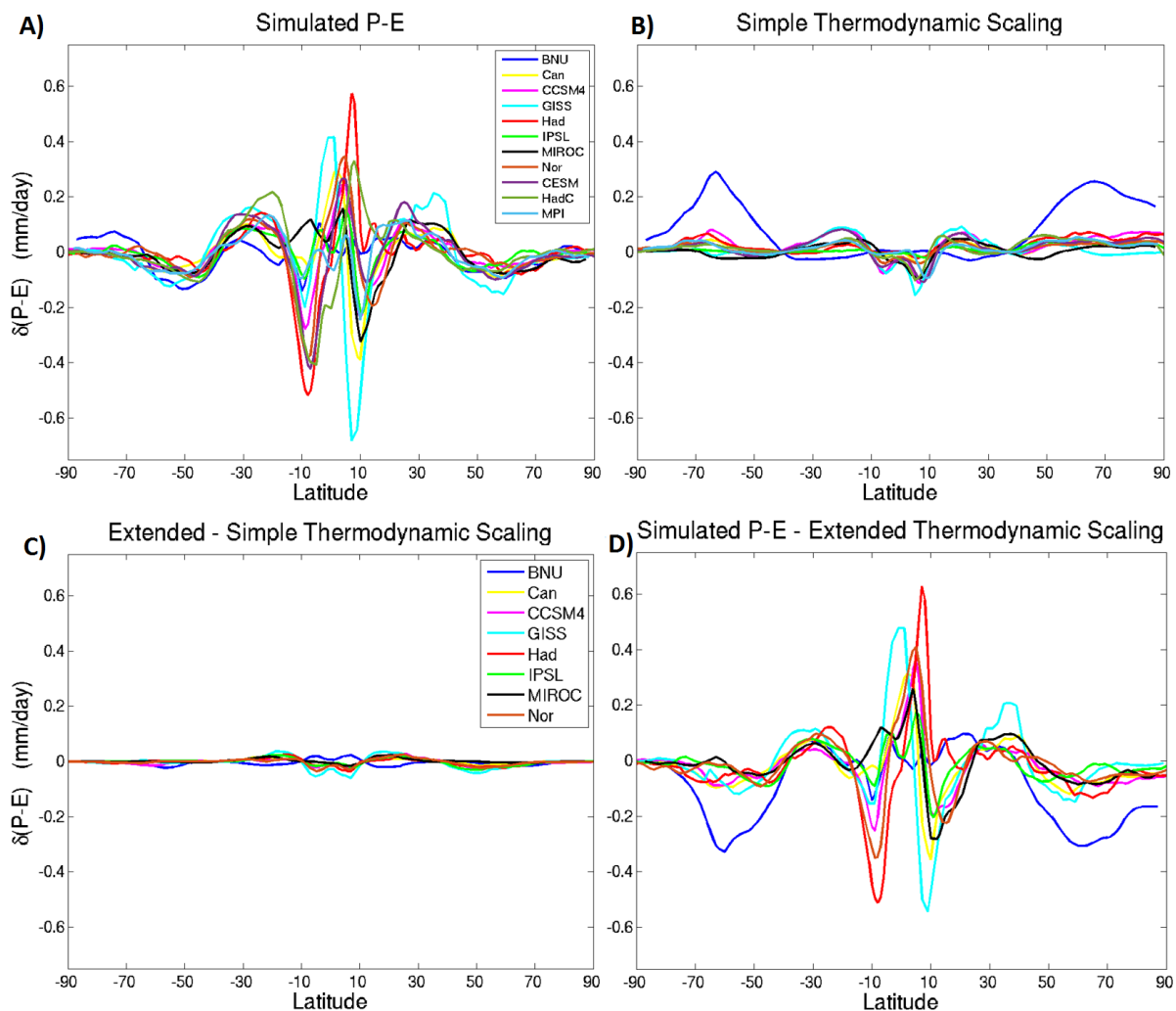


Figure 4. A) shows the zonal mean P-E in eleven climate models as simulated in the models, and B) is the P-E predicted by the simple thermodynamic scaling in Eq. (2). C) shows the difference between the extended (Eq. (3)) and simple (Eq. (2)) scalings. This isolates the contribution of local relative humidity changes to the P-E anomalies. D) is the difference between the simulated P-E and the extended scaling, and represents the changes in dynamically driven rainfall. (EC-Earth excluded due to unphysical result).



Ensemble Mean δ Relative Humidity, G1-Preindustrial (%)

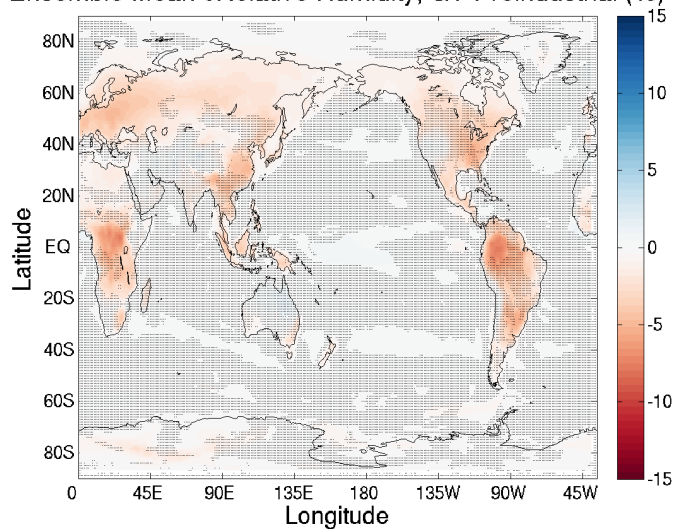


Figure 5. The annual mean near-surface relative humidity anomaly between G1 (years 11-50) and the Preindustrial Control (all years) in eight GCMs. Stippling indicates that fewer than 62.5% of the models agree on the sign of the change. (Data unavailable for HadC, CESM, and MPI models; EC-Earth excluded).

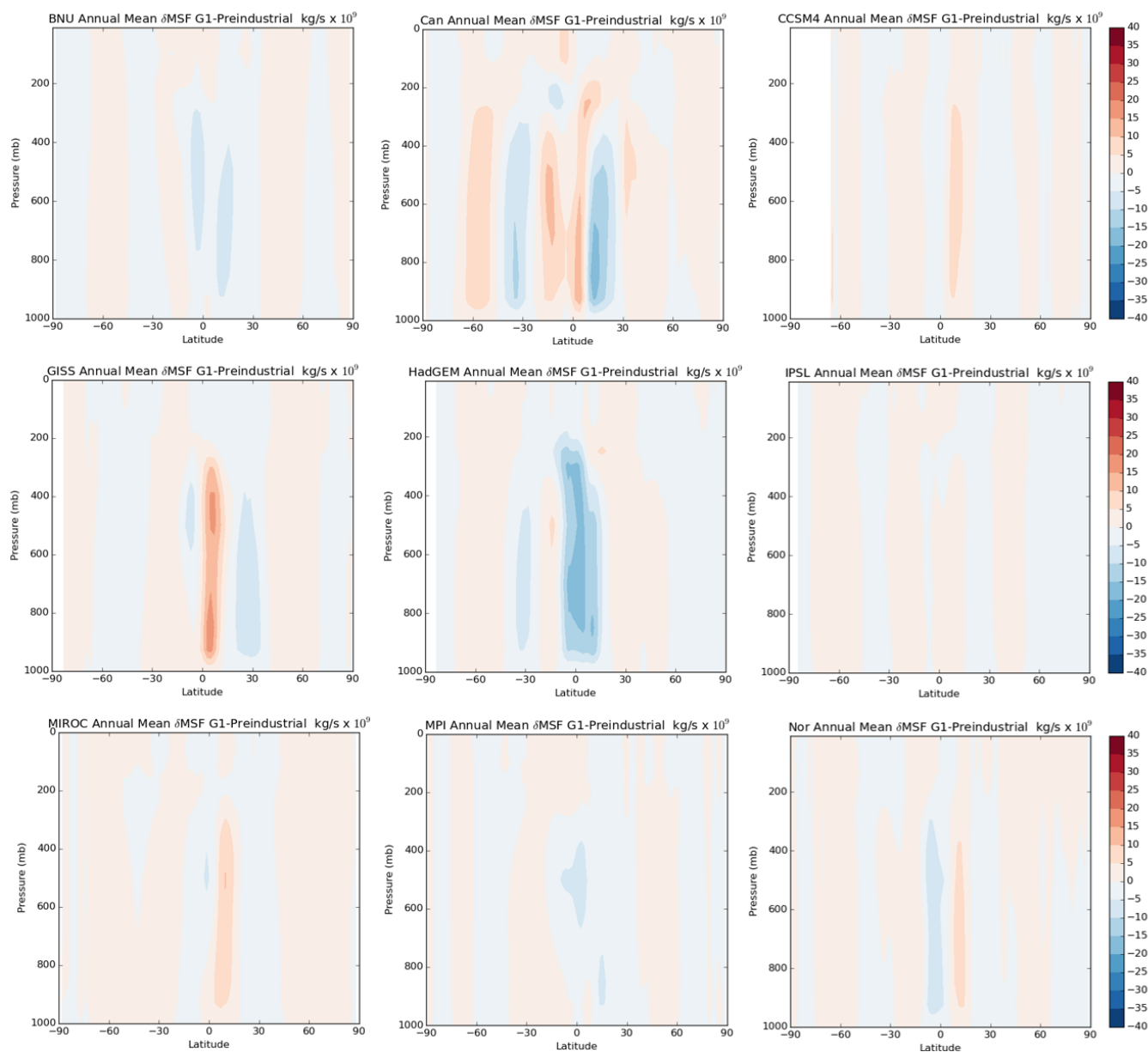


Figure 6. The annual mean meridional streamfunction anomaly between G1 (years 11-50) and the Preindustrial Control (last 40 years) in each model, as calculated in Eq. (4). Blue colors indicate counterclockwise motion. (Data unavailable for HadC and CESM models).

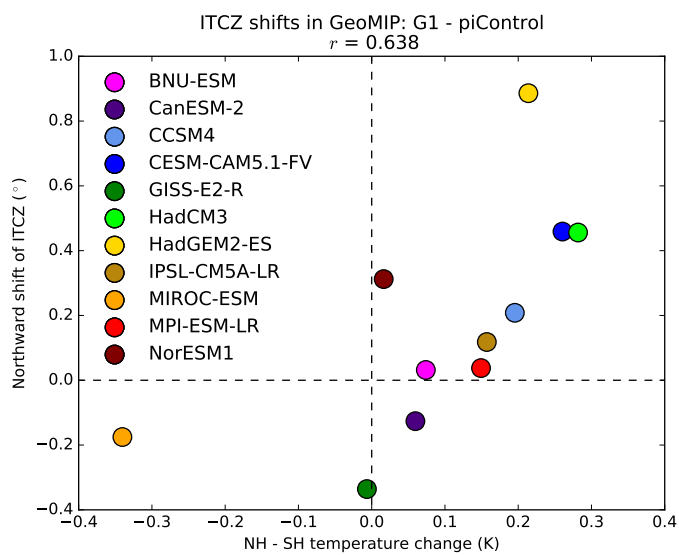


Figure 7. The ITCZ shift vs. the anomaly of the interhemispheric temperature contrast between G1 (years 11-50) and the Preindustrial Control (years 1-40).



Table 1. GeoMIP Model Specifications. In certain figures models are labeled with the shortened name in parenthesis. Column 3 refers to the CO_2 physiological effect in plants. The S_0 reduction is a percentage. Information courtesy of Kravitz et al. 2013a

Model ¹	Dynamic Vegetation	Phys. Effect	S_0 Reduction
BNU-ESM (BNU)	no	yes	3.8
Can-ESM2 (Can)	yes	yes	4.0
CESM-CAM5.1-FV (CESM)	no	yes	4.7
CCSM4 (CCSM4)	no	yes	4.1
EC-Earth	N/A	no	4.3
GISS-E2-R (GISS)	no	yes	4.5
HadCM3 (HadC)	no	yes	4.1
HadGEM2-ES (Had)	yes	yes	3.9
IPSL-CM5A-LR (IPSL)	yes	yes	3.5
MIROC-ESM (MIROC)	yes	yes	5.0
MPI-ESM-LR (MPI)	no	yes	4.7
NorESM1-M (Nor)	no	yes	4.0

1. Full Names: BNU-ESM, Beijing Normal University-Earth System Model; CanESM2, The Second Generation Canadian Earth System Model; CESM-CAM5.1, The Community Climate System Model Version 5.1; CCSM4, The Community Climate System Model Version 4; EC-EARTH DMI, European Earth System Model based on ECMWF Models (Seasonal Forecast System), Danish Meteorological Institute; GISS-E2-R, Goddard Institute for Space Studies ModelE version 2; HadCM3, Hadley Centre coupled model 3; IPSL-CM5A-LR, Institut Pierre Simon Laplace ESM; MIROC-ESM, Model for Interdisciplinary Research on Climate-Earth System Model; MPI-ESM-LR, Max Planck Institute ESM; NorESM1-M, Norwegian ESM.